iScience

CellPress
OPEN ACCESS

Article

Mitochondria-targeted cancer analysis using survival and expression: Prioritizing mitochondrial targets that alleviate pancreatic cancer cell phenotypes

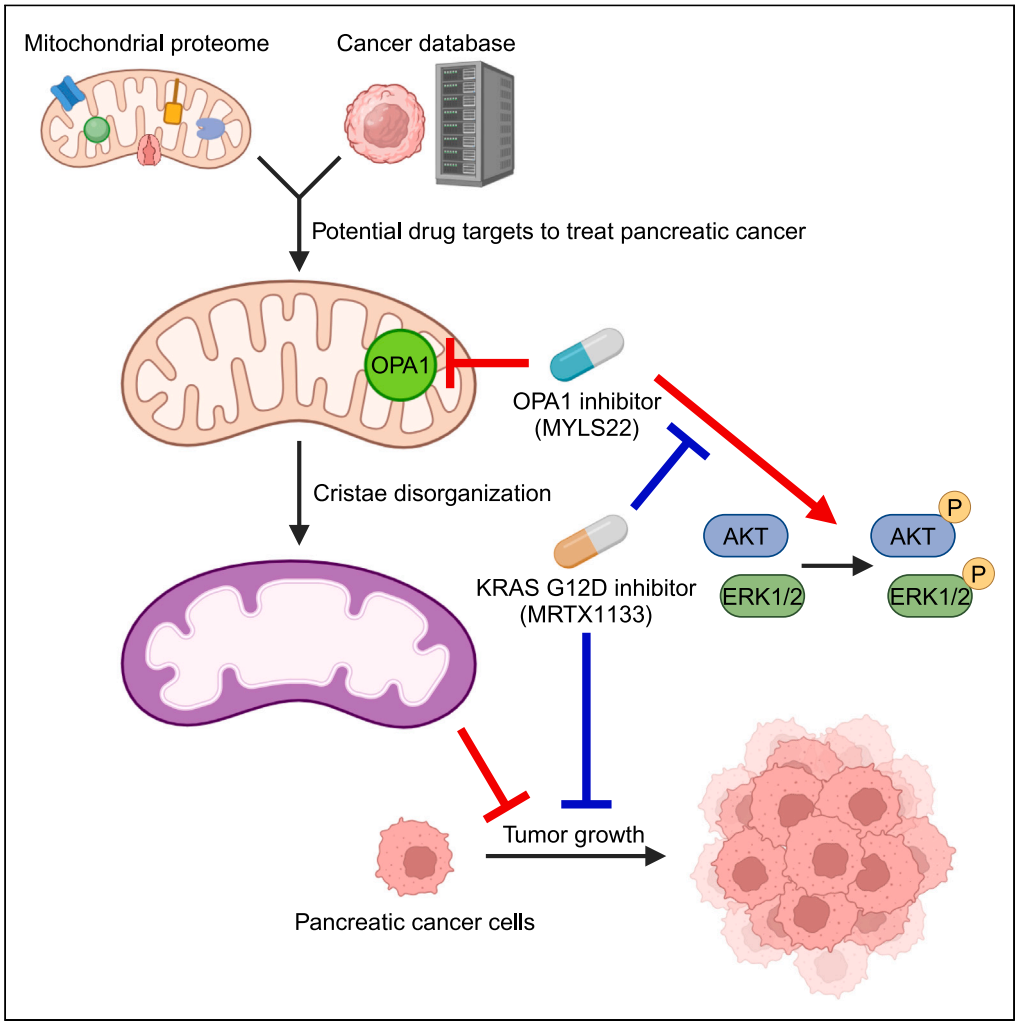

Daisuke Murata, Fumiya Ito, Gongyu Tang, ..., Xiaowei Wang, Miho Iijima, Hiromi Sesaki

miijima@jhmi.edu (M.I.)
hsesaki@jhmi.edu (H.S.)

Highlights

We developed a method to identify mitochondrial targets for mitigating cancer

OPA1 inhibition suppresses pancreatic cancer phenotypes

Cristae integrity is crucial for pancreatic cancer cell proliferation

OPA1 and KRAS inhibitors synergistically inhibit pancreatic cancer cells

Murata et al., iScience 27, 110880
September 20, 2024
https://doi.org/10.1016/j.isci.2024.110880

iScience

CellPress
OPEN ACCESS

Article

Mitochondria-targeted cancer analysis using survival and expression: Prioritizing mitochondrial targets that alleviate pancreatic cancer cell phenotypes

Daisuke Murata,[1] Fumiya Ito,[1] Gongyu Tang,[2,3] Wakiko Iwata,[1] Nelson Yeung,[1] Junior J. West,[1] Andrew J. Ewald,[1,4,5,6] Xiaowei Wang,[2,3] Miho Iijima,[1,*] and Hiromi Sesaki[1,7,*]

SUMMARY

Substantial changes in energy metabolism are a hallmark of pancreatic cancer. To adapt to hypoxic and nutrient-deprived microenvironments, pancreatic cancer cells remodel their bioenergetics from oxidative phosphorylation to glycolysis. This bioenergetic shift makes mitochondria an Achilles' heel. Since mitochondrial function remains essential for pancreatic cancer cells, further depleting mitochondrial energy production is an appealing treatment target. However, identifying effective mitochondrial targets for treatment is challenging. Here, we developed an approach, mitochondria-targeted cancer analysis using survival and expression (mCAUSE), to prioritize target proteins from the entire mitochondrial proteome. Selected proteins were further tested for their impact on pancreatic cancer cell phenotypes. We discovered that targeting a dynamin-related GTPase, OPA1, which controls mitochondrial fusion and cristae, effectively suppresses pancreatic cancer activities. Remarkably, when combined with a mutation-specific KRAS inhibitor, OPA1 inhibition showed a synergistic effect. Our findings offer a therapeutic strategy against pancreatic cancer by simultaneously targeting mitochondria dynamics and KRAS signaling.

INTRODUCTION

Pancreatic cancer is the fourth leading cause of cancer-associated death, with high levels of metastasis.[1–6] Its average 5-year survival rate is approximately 10%, and with predicted increases in its occurrence, pancreatic cancer is estimated to become the second leading cause of cancer-associated death by 2030.[7] Current therapies are not effective enough for patients with pancreatic cancer. There is an urgent need to identify therapeutic interventions for this devastating cancer.

Genetic mutations predominantly drive pancreatic cancer tumorigenesis and progression, especially in the four major oncogenes and tumor suppressors: KRAS, p16/CDKN2A, TP53, and DPC4/SMAD4.[1–4] KRAS mutations are one of the earliest critical events in the development of pancreatic cancer and occur in more than 80% of cases.[1–4] Downstream signaling of KRAS is mediated by two major protein kinases, ERK and AKT, which control cell proliferation and metastasis. In addition to intracellular signal transduction, during the development of pancreatic cancer, cellular energy metabolism shifts from oxidative phosphorylation to glycolysis to fuel rapid and massive cancer cell proliferation.[8–10] Notably, even after an increase in glycolysis, oxidative phosphorylation remains essential for generating ATP in pancreatic cancer, albeit at a reduced rate, to ensure the growth and viability of cancer cells.[9–12] These unique bioenergetic characteristics present an excellent opportunity to target mitochondria as a therapeutic strategy against pancreatic cancer.[9–12] Since the mitochondrial proteome contains more than 1000 proteins,[13] identifying effective targets poses a significant challenge to developing mitochondria-focused strategies to alleviate pancreatic cancer.

In this study, we address this challenge by introducing a method termed Mitochondria-targeted Cancer Analysis Using Survival and Expression (mCAUSE). This method prioritizes target proteins based on their gene expression levels and correlation with the survival rates of patients with pancreatic cancer.

[1]Department of Cell Biology, Johns Hopkins University School of Medicine, Baltimore, MD, USA
[2]Department of Pharmacology and Regenerative Medicine, University of Illinois Chicago, Chicago, IL, USA
[3]University of Illinois Cancer Center, University of Illinois Chicago, Chicago, IL, USA
[4]Department of Oncology, Sidney Kimmel Comprehensive Cancer Center, Johns Hopkins University School of Medicine, Baltimore, MD, USA
[5]Giovanis Institute for Translational Cell Biology, Johns Hopkins University School of Medicine, Baltimore, MD, USA
[6]Department of Biomedical Engineering, Johns Hopkins University Whiting School of Engineering, Baltimore, MD, USA
[7]Lead contact
*Correspondence: miijima@jhmi.edu (M.I.), hsesaki@jhmi.edu (H.S.)
https://doi.org/10.1016/j.isci.2024.110880

RESULTS

Development of mitochondria-targeted cancer analysis using survival and expression

To understand how the survival of patients with pancreatic cancer is correlated with the expression of genes that encode mitochondrial proteins (termed mito-genes), we first retrieved all 1136 mito-genes listed in human MitoCarta3.0[13] (Figure 1A). Using the Cancer Genome Atlas (TCGA)[14] and OncoDB,[15] we divided the cancer cases into a "high" or "low" expression group for each mito-gene based on a median 50% threshold of mRNA levels (Table S1, Total analyzed). The analysis excluded 13 mitochondrial DNA-encoded genes that were not included in the NCBI RefSeq curated database, as well as 7 nuclear DNA-encoded genes that were not part of OncoDB. We then utilized a log rank test to compare the survival between these two groups. This analysis revealed that 219 mito-genes are linked to significant changes in patient survival (Table S1, HR altered). Of these 219, higher levels of 45 mito-genes were associated with compromised survival (Hazard Ratio >1, Blue line, Figure 1A) (Table S1, HR > 1). In contrast, higher levels of 174 mito-genes were associated with better survival (Hazard Ratio <1, Red line, Figure 1A) (Table S1, HR < 1).

To determine whether and how the expression of these 219 genes is altered in pancreatic cancer compared to normal tissues, we analyzed individual mRNA levels and grouped them into four categories using TCGA and OncoDB (Table S2). In the group of 45 mito-genes with a hazard ratio greater than 1, the expression of 39 of these genes was significantly altered, showing a more than 2-fold increase compared to normal tissues. All of these genes were upregulated in tumors (Figure 1A, Category A) (Table S3). We were most interested in this first category (A); these genes potentially exhibit oncogenic properties, and lowering their expression or inhibiting their function might mitigate pancreatic cancer. Therefore, these mito-genes are strong candidates for drug targets to treat pancreatic cancer. However, it should also be noted that such increased levels may be the consequence of other changes in tumors. Gene ontology (GO) analysis showed that two pathways are significantly enriched, including mitochondrial translation (nine genes) and mitochondrial membrane organization (five genes) (Figure 1A) (Table S4). The second category (B) describes genes that are significantly decreased in their expression levels by more than half, yet higher expression levels are associated with poor survival. We expected to find fewer genes in this category as the expression-survival relationship appears somewhat conflicting. Indeed, we found no mito-genes in this category (Figure 1A).

In the group of 174 mito-genes with a hazard ratio smaller than 1, the expression of 89 mito-genes was significantly altered by greater than 2-fold compared to normal tissues. The third category (C) contains 72 genes that are higher in their expression in pancreatic cancer (Figure 1A) (Table S4). GO analysis indicated that three pathways are significantly enriched, including the regulation of mitochondrial translation (four genes), mitochondrial electron transport chain complex I assembly (nine genes), and mitochondrial RNA metabolic processes (five genes) (Table S4). The fourth category (D) has genes that are lower in expression, but increased levels are linked to better survival (Figure 1A) (Table S4). Seventeen mito-genes were found in this category. We consider that these genes might function as tumor suppressors. While these correlations may be secondary consequences of pancreatic cancer, it is also possible that boosting their function would decrease pancreatic cancer growth or improve patient survival. GO analysis revealed one pathway significantly enriched in this category: mitochondrial gene expression (four genes). Thus, mCAUSE divided mito-genes into four categories, identifying 39 genes with potential oncogenic features (category A) and 17 genes that may function such as tumor suppressors (category D).

Evaluation of mitochondria-targeted cancer analysis using survival and expression

To evaluate the usefulness of mCAUSE, we tested the impact of the identified genes on pancreatic cancer cells. Specifically, we focused on the genes in category (A), which show potential oncogenic characteristics, using two pancreatic cancer cell lines with different genetic makeups: PANC-1 and MIA PaCa-2 cells (Figures 1B and 1C). We blocked two enriched pathways — mitochondrial translation by chloramphenicol and mitochondrial membrane organization by MYLS22[16,17] (which inhibits OPA1, a mitochondrial dynamin-related GTPase that controls mitochondrial fusion and cristae structure). We also inhibited gene products in category (A) that available drugs can pharmacologically target. These inhibitors include R162[18] to inhibit the glutamate dehydrogenase GLUD1, YMU1[19] to inhibit thymidylate kinase DTYMK, BI-6C9[20] to inhibit the apoptotic protein BID, AP5A to inhibit adenylate kinase AK4, Fidarestat to inhibit the aldo-keto reductase AKR1B10, ML348 to inhibits the lysophospholipase LYPLA1, and FC9402 to inhibit the sulfide quinone oxidoreductase SQOR. We used concentrations commonly employed for each chemical. PANC-1 and MIA PaCa-2 cells were cultured for 48 h in the presence of these inhibitors and analyzed for their cell density using crystal violet staining (Figures 1B and 1C). We found that the OPA1 inhibitor MYLS22 induces a significant and large decrease in cell density in both PANC-1 and MIA PaCa-2 cells. In contrast, the mitochondrial translation inhibitor chloramphenicol induced modest reductions in cell density only in MIA PaCa-2 cells. Other inhibitors did not decrease cell density in either cell line.

MYLS22 blocks mitochondrial fusion and disorganizes cristae

As described above, OPA1 controls mitochondrial fusion and cristae formation.[21] To confirm the effect of MYLS22 on these processes in PANC-1 cells, we analyzed mitochondrial morphology, dynamics, and ultrastructure. First, PANC-1 cells were treated with MYLS22 for 24 h and subjected to laser confocal immunofluorescence microscopy using antibodies against the mitochondrial protein pyruvate dehydrogenase (PDH) (Figures 2A and 2B). In control cells, mitochondria displayed short tubular structures with occasional branches. In contrast, MYLS22-treated cells contained highly fragmented, small mitochondria (Figures 2A and 2B). Mitochondrial fragmentation likely results from decreased mitochondrial fusion, leading to unopposed, excess mitochondrial division. Second, to more directly test whether MYLS22 suppresses mitochondrial fusion in PANC-1 cells, we utilized a mitochondrial fusion assay involving live-cell imaging with matrix-targeted photoactivatable GFP (mitoPAGFP), as we performed[22] (Figures 2C and 2D). PANC-1 cells were infected with lentiviruses carrying mitoPAGFP and treated with MYLS22 for 24 h. Following treatment, the cells were stained with tetramethylrhodamine ethyl ester (TMRE) to

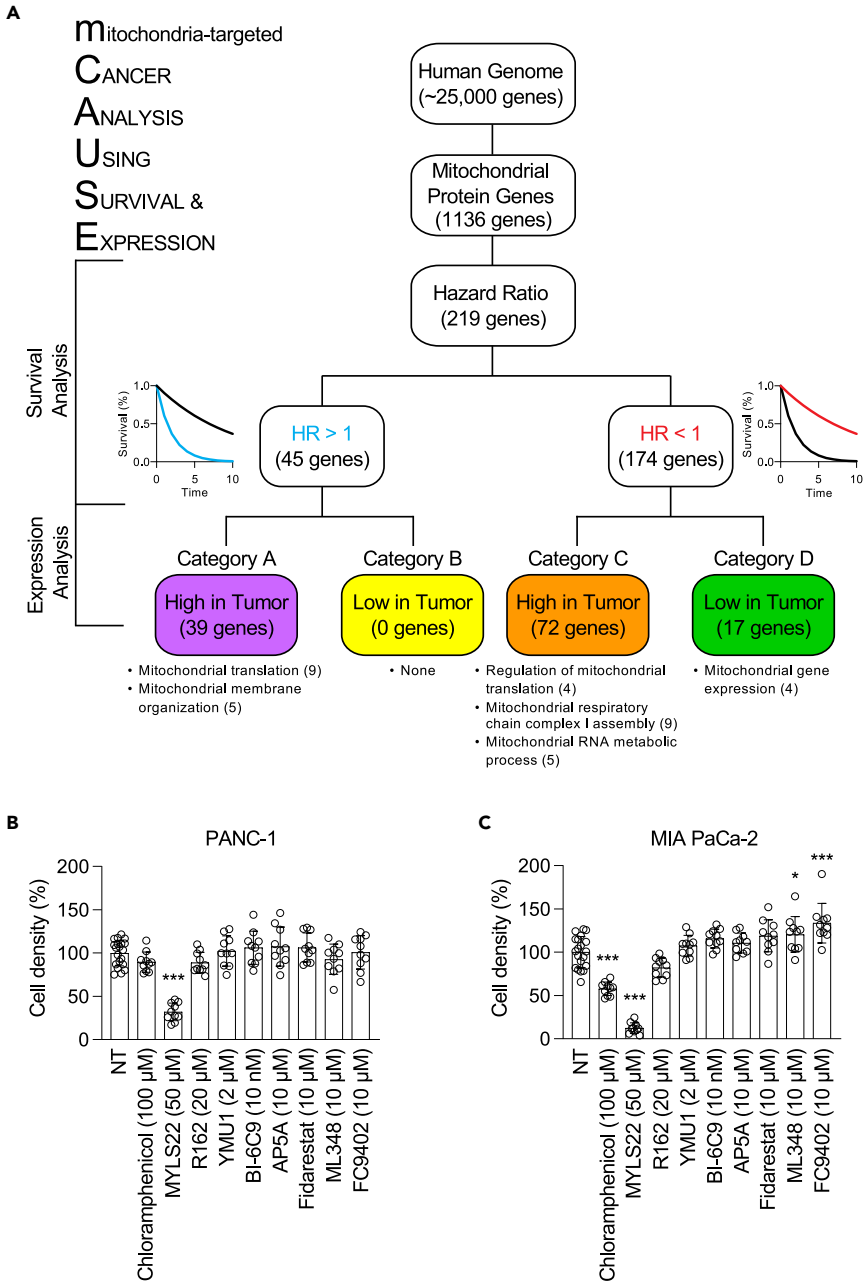

Figure 1. Mitochondria-targeted cancer analysis using survival and expression

(A) Out of 25,000 proteins in the human proteome, MitoCarta3.0 identified 1136 mitochondrial proteins. Of these, 219 mito-genes exhibited a significant difference in hazard ratio (HR). Specifically, 45 mito-genes were associated with decreased survival in patients with pancreatic cancer when expressed at increased levels. Among these, category A includes 39 genes expressed at higher levels in tumors than in normal tissues. In contrast, when expressed at increased levels, 174 mito-genes were associated with better survival. Category C includes 72 of these genes that are also expressed at higher levels in tumors, while category D comprises 17 genes that are expressed at lower levels in tumors. GO enrichment analysis was performed by PANTHER with Bonferroni correction. Biological processes with a *p*-value less than 0.05 and greater than 20-fold enrichment are presented.

(B and C) PANC-1 cells (B) and MIA PaCa-2 cells (C) were cultured in the presence of the indicated inhibitors for 72 h. Cell density was determined using a crystal violet assay (mean ± SD, $n \geq 10$). ANOVA with post-hoc Tukey: *$p < 0.05$, ***$p < 0.001$.

visualize the entire mitochondrial network. After the photoactivation of mitoPAGFP in a small portion of the mitochondria, we monitored the mixing of the fluorescent matrix marker through mitochondrial fusion. In control PANC-1 cells, the fluorescence intensity of mitoPAGFP gradually decreased over 60 min to approximately 40% of the initial intensity (Figures 2C and 2D). In contrast, treatment with MYLS22 significantly

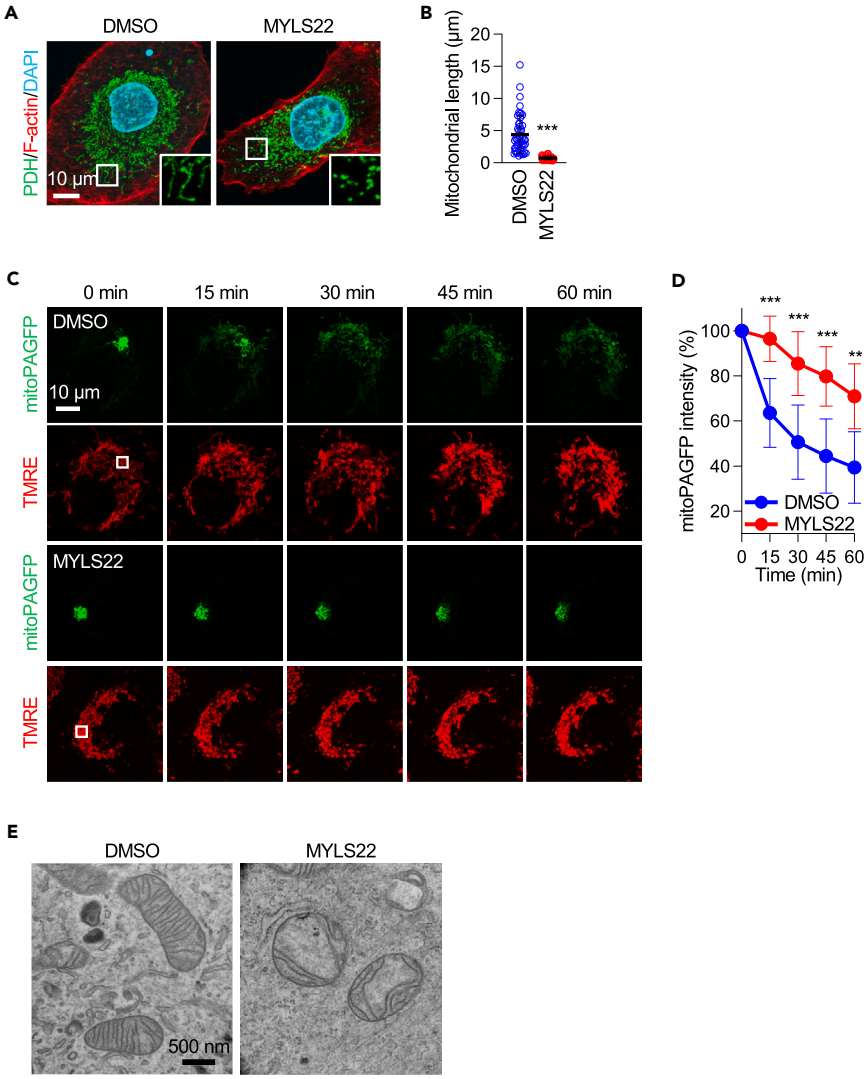

Figure 2. MYLS22 blocks mitochondrial fusion and disorganizes inner membrane cristae

(A) Mitochondrial morphology. PANC-1 cells were treated with DMSO or MYLS22 for 24 h and subjected to laser confocal immunofluorescence microscopy with anti-PDH antibodies. The boxed regions are magnified.

(B) Quantification of mitochondrial length (mean ± SD, $n = 50$).

(C) Mitochondrial fusion. PANC-1 cells expressing mitoPAGFP were incubated with DMSO or MYLS22 for 24 h. Subsequently, cells were stained with 5 nM TMRE. MitoPAGFP was photoactivated using a 405 nm laser in a small region indicated by a square at 0 min. Observations were made at 15-min intervals over 60 min.

(D) The fluorescence intensity of mitoPAGFP in the photoactivated region was quantified (mean ± SD, $n > 9$).

(E) PANC-1 cells were treated with DMSO or MYLS22 for 24 h and subjected to transmission electron microscopy. Student's t-test in (B) and ANOVA followed by Šídák's test in (D): $^{**}p < 0.01$, $^{***}p < 0.001$.

slowed the diffusion of the photoactivated mitoPAGFP among mitochondria. These data show that MYLS22 effectively decreases mitochondrial fusion. Third, to determine if MYLS22 affects cristae structure in PANC-1 cells, we performed transmission electron microscopy. In control cells, the mitochondrial inner membrane displayed well-developed cristae structures (Figure 2E). In contrast, cells treated with MYLS22 showed reduced and disorganized cristae (Figure 2E). Taken together, these data indicate that MYLS22 effectively inhibits mitochondrial fusion and cristae formation.

Inhibiting normal cristae formation, but not mitochondrial fusion, suppresses cell proliferation

To determine which function of OPA1 is critical for suppressing cell proliferation in PANC-1 cells, we knocked down another dynamin-related GTPase, MFN1, which mediates mitochondrial fusion but not cristae formation, using two different siRNAs. Western blotting showed a significant reduction in MFN1 protein levels by these siRNAs (Figures 3A and 3B). Immunofluorescence microscopy showed the fragmentation of

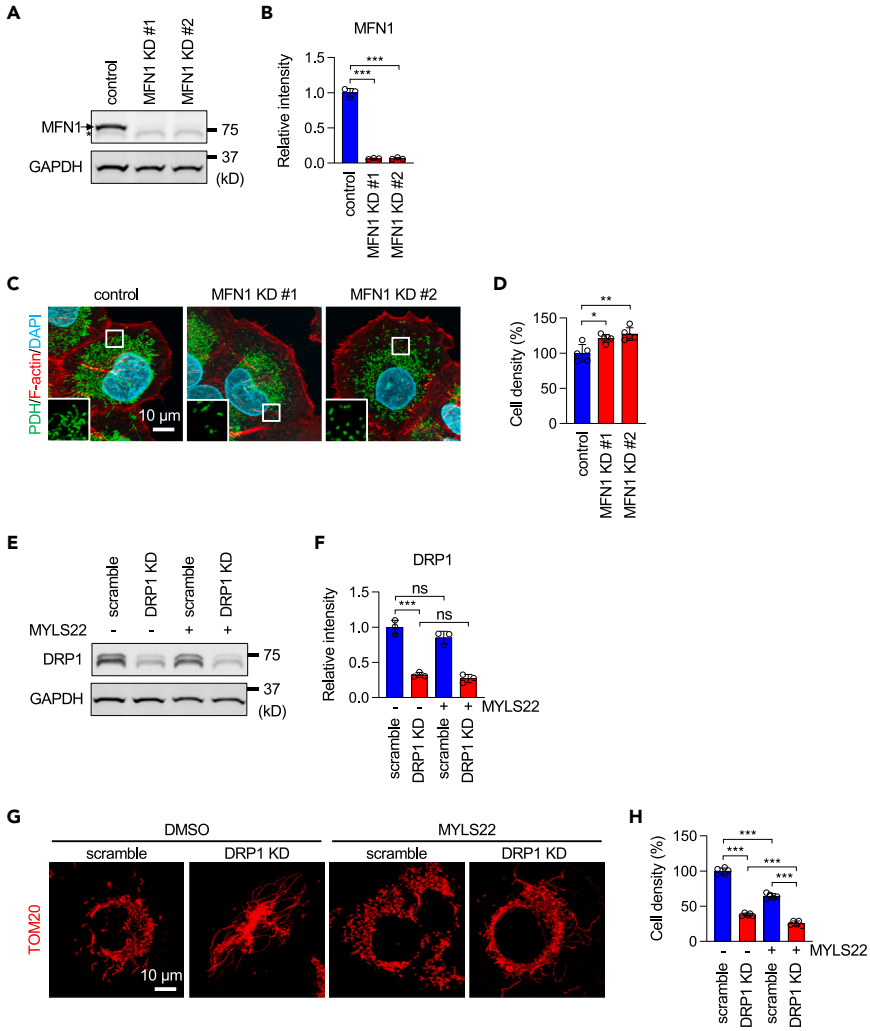

Figure 3. Mitochondrial fusion is dispensable for cell proliferation

(A) Western blotting of PANC-1 cells treated with non-targeting control or two different MFN1 siRNAs for 5 days. An arrow and an asterisk indicate MFN1 and non-specific bands, respectively.

(B) Quantification of band intensity (mean ± SD, $n = 3$).

(C) PANC-1 cells were transfected with the indicated siRNAs and subjected to laser confocal immunofluorescence microscopy with anti-PDH antibodies. The boxed regions are magnified.

(D) Cell proliferation of the transfectants was examined by a crystal violet assay (mean ± SD, $n = 5$).

(E) PANC-1 cells were infected with lentiviruses expressing scramble or DRP1 shRNAs and then treated with DMSO or MYLS22 for 24 h. Knockdown of DRP1 was confirmed by Western blotting.

(F) Quantification of band intensity (mean ± SD, $n = 3$).

(G) Mitochondria were analyzed by immunofluorescence microscopy with anti-TOM20 antibodies.

(H) Cell proliferation was analyzed by a crystal violet assay (mean ± SD, $n = 5$). ANOVA with post-hoc Tukey in (B, D, F, H): $*p < 0.05$, $***p < 0.01$, $***p < 0.001$.

mitochondria due to the inhibition of mitochondrial fusion (Figure 3C). However, MFN1 knockdown did not reduce PANC-1 cell proliferation (Figure 3D). These data suggest that mitochondrial fusion is dispensable for the proliferation of PANC-1 cells.

To further confirm this notion, we blocked mitochondrial division by using shRNA knockdown of DRP1 in PANC-1 cells treated with MYLS22 (Figures 3E and 3F). We found that mitochondrial fragmentation is rescued by DRP1 knockdown (Figure 3G). However, rescuing mitochondrial fragmentation failed to rescue cell proliferation defects caused by MYLS22: knockdown of DRP1 decreased cell proliferation, consistent with a previous study,[23] and the combination of DRP1 knockdown and MYLS22 showed further reduction (Figure 3H).

To test the effect of cristae formation inhibition, we knocked down MIC60, a vital component of the MICOS complex responsible for cristae formation,[24,25] using two different siRNAs. We confirmed the knockdown using Western blotting (Figures 4A and 4B). Electron microscopy showed the loss of normal cristae structure in MIC60 knockdown cells, consistent with previous reports[24,25] (Figure 4C). MIC60 knockdown

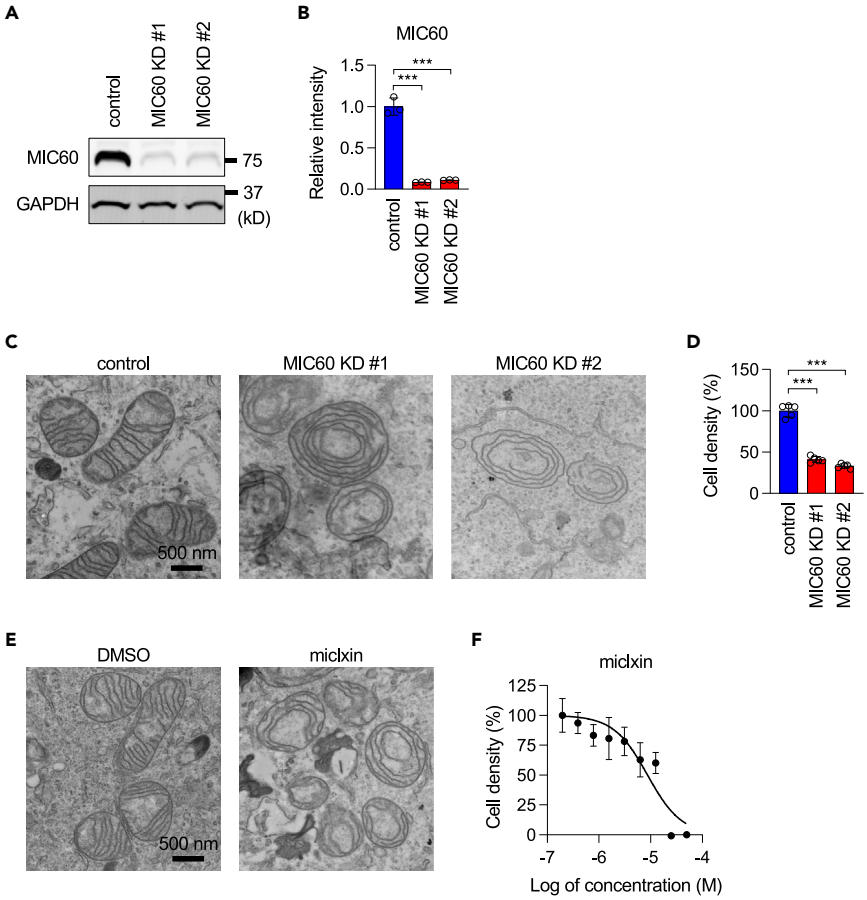

Figure 4. Cristae are important for cell proliferation

(A) Western blotting of PANC-1 cells treated with non-targeting control or two different MIC60 siRNAs for 5 days.

(B) Quantification of band intensity (mean ± SD, $n = 3$).

(C) Mitochondria were analyzed in PANC-1 cells transfected with the indicated siRNAs by electron microscopy.

(D) PANC-1 cells were transfected with the indicated siRNAs. Cell proliferation was assessed using a crystal violet assay (mean ± SD, $n = 5$).

(E) Mitochondria were analyzed in PANC-1 cells treated with DMSO or 10 μM miclxin by electron microscopy.

(F) PANC-1 cells were cultured with 0–50 μM miclxin for 72 h. Cell density was assessed using a crystal violet assay (mean ± SD, $n = 5$). ANOVA with post-hoc Tukey in (B, D): ***$p < 0.001$.

resulted in significant decreases in cell proliferation for both siRNAs (Figure 4D). Furthermore, we treated PANC-1 cells with a MIC60 inhibitor, miclxin.[26] Results showed that miclxin disorganizes inner membrane cristae (Figure 4E) and blocks cell proliferation in a dose-dependent manner (Figure 4F). These data suggest that cristae morphology plays a crucial role in the proliferation of PANC-1 cells.

MYLS22 decreases mitochondrial respiration

Since cristae are important for efficient mitochondrial oxidative phosphorylation, we investigated how MYLS22 affects oxygen consumption rates (OCRs) in PANC-1 cells. We found that MYLS22 strongly decreases both basal OCRs and respiratory capacity (Figures 5A–5C). Since reduced mitochondrial energy production can lead to a compensatory upregulation of glycolysis, we also measured the extracellular acidification rates (ECARs) for glycolysis. Indeed, we observed an increase in glycolysis in MYLS22-treated PANC-1 cells (Figures 5D and 5E). This increase did not affect glycolytic capacity or reserve (Figures 5F and 5G). Therefore, MYLS22 decreases mitochondrial respiration but not cytosolic glycolysis in PANC-1 cells.

MYLS22 decreases spheroid growth and cell motility

To further analyze the impact of MYLS22 on pancreatic cell phenotypes, we utilized a three-dimensional spheroid growth model, which closely represents physiological conditions.[27] We generated spheroids of PANC-1 cells using the hanging drop method and placed the spheroids in a 3D meshwork of the extracellular matrix using Geltrex.[27] Control spheroids showed substantial growth at 5 days and invasion at 7 days (Figures 6A and 6B). In contrast, spheroids treated with MYLS22 displayed significantly decreased growth and no invasion. Inhibition of

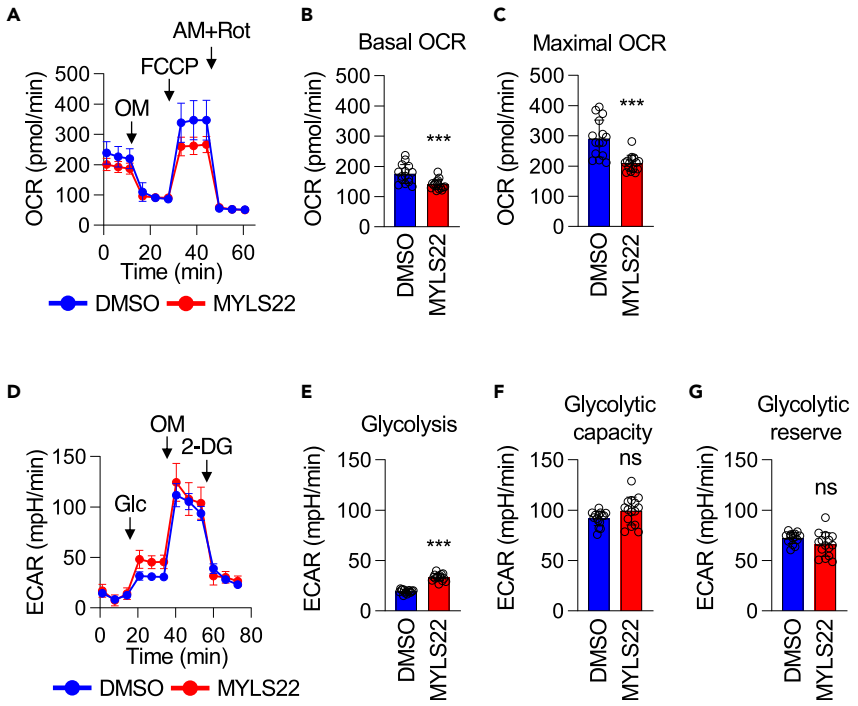

Figure 5. MYLS22 alters energy metabolism

(A) Mitochondrial respiration was analyzed by measuring the OCRs in PANC-1 cells treated with MYLS22.

(B and C) Both basal and maximal OCRs are presented (mean ± SD, $n = 15$).

(D–G) Glycolysis was assessed by measuring the ECARs in the same set of cells. Basal glycolysis (E), glycolytic capacity (F), and glycolytic reserve (G) are shown (mean ± SD, $n = 13$). Student's t-test in (B, C, E, F, G): ***$p < 0.001$.

invasion in spheroids by MYLS22 (Figures 6A and 7 days) suggested that MYLS22 suppresses migratory activities of PANC-1 cells. To directly test this notion, we examined cell motility using a wound-healing assay (Figures 6C and 6D). In this assay, we plated cells and cultured them to 100% confluency. Then, a line of scratches was made with small pipette tips. The migration of cells into the scratched width was monitored over 72 h in the presence or absence of 50 μM MYLS22. MYLS22 significantly decreased cell migration (Figures 6C and 6D).

MYLS22 stimulates the phosphorylation of AKT and ERK

Mutated, constitutively active KRAS mutations are the primary driver of pancreatic cancer.[1–4] Activated KRAS signaling promotes mitochondrial division by phosphorylating the division GTPase DRP1 through one of the major downstream kinases, ERK1/2.[28,29] However, the functional relationships between the fusion GTPase OPA1 and the KRAS pathway are not well understood. Therefore, we were interested in determining if MYLS22 affects this oncogenic pathway. Since the phosphorylation of ERK1/2 and AKT are two major downstream events in the KRAS signaling pathway, we tested whether these phosphorylation events are affected by MYLS22. Specifically, we examined ERK 1/2 phosphorylation at Thr202/Tyr204 and AKT phosphorylation at Ser473 and Thr308[30–33] (Figures 7A and 7B). We found a significant increase in the phosphorylation of both ERK1/2 and AKT following MYLS22 treatment (Figures 7A and 7B).

To determine whether the increased phosphorylation of ERK1 and AKT is dependent on KRAS, we added MRTX1133, an allele-specific KRAS inhibitor targeting the oncogenic G12D mutation, along with MYLS22, as PANC-1 cells carry this KRAS mutation.[34] The G12D mutation is the most frequent KRAS mutation, accounting for approximately 40% of pancreatic cancer cases. MRTX1133 is currently undergoing Phase 2 clinical trials for the treatment of solid tumor malignancies harboring this mutation, including pancreatic cancer. We found that MRTX1133 strongly blocks ERK1/2 phosphorylation induced by MYLS22 (Figures 7A and 7B). AKT phosphorylation was also suppressed by MRTX1133 (Figures 7A and 7B). These results indicate that MYLS22 affects KRAS signaling in PANC-1 cells. The elevated levels of ERK1/2 and AKT phosphorylation by MYLS22 may be an adoptive response to the decreased cell proliferation and migration resulting from mitochondrial deficits.

Effects of combined treatments with MYLS22 and MRTX1133 on cell proliferation and spheroid growth

If increased KRAS signaling is a compensatory mechanism in the presence of OPA1 inhibition, concurrently inhibiting OPA1 and KRAS signaling could be an effective strategy against pancreatic cancer cells. To test our hypothesis, we treated PANC-1 cells with MRTX1133 in the presence or absence of MYLS22. First, we confirmed that MRTX1133 inhibits the proliferation of PANC-1 cells in a dose-dependent manner (Figure 8A) and determined its IC_{50} to be approximately 30 μM (Figure 8C). To test whether the presence of MYLS22 changes the

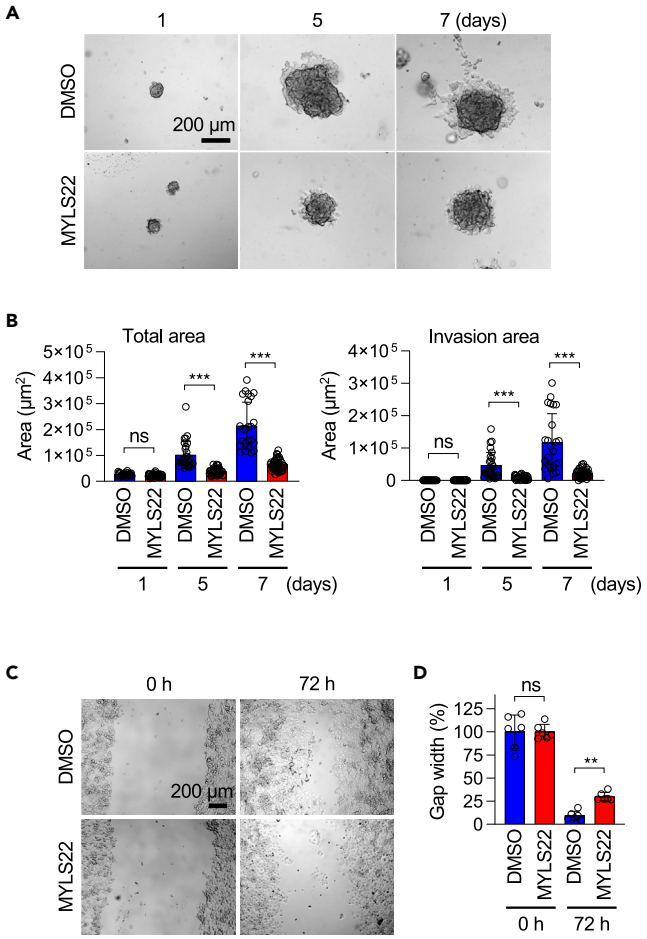

Figure 6. OPA1 inhibition suppresses spheroid growth and cell migration

(A) Spheroid growth. Spheroids of PANC-1 cells were cultured in Geltrex for 7 days in the presence of DMSO or 50 µM MYLS22.

(B) Quantification of the total and invasion areas (mean ± SD, $n > 20$).

(C) Cell migration. Motility of PANC-1 cells was analyzed using a wound-healing assay. Representative images at 0 h and 72 h are shown.

(D) Wound closure was assessed by determining the relative width over the initial width (mean ± SD, $n = 5$). Student's t-test in (B, D): $^{**}p < 0.01$, $^{***}p < 0.001$.

IC_{50} of MRTX1133, we included a sub-effective concentration of MYLS22 (12.5 µM, Figure 8B, arrow) and found that 12.5 µM MYLS22 significantly decreases the IC_{50} of MRTX1133 in the proliferation of PANC-1 cells (Figure 8C). These data suggest that MRTX1133 and MYLS22 have a synergistic effect on cell proliferation. To further explore the combined effects of MRTX1133 and MYLS22, we incubated the spheroids with low doses of MRTX1133 (4 nM) and MYLS22 (1 µM). At these concentrations, individual drug treatments showed no significant effects on the growth or invasion of spheroids (Figures 8D and 8E). In contrast, the combination of these drugs demonstrated synergistic effects in inhibiting spheroid growth and dissemination (Figures 8D and 8E). These data taken together suggest that combining the inhibition of KRAS and OPA1 provides an effective strategy to counteract pancreatic cancer phenotypes.

DISCUSSION

In the current work, we have developed mCAUSE, a method to identify mitochondrial proteins that could be targeted to mitigate phenotypes in cancer cells. This identification is based on a correlation analysis between patient survival and gene expression using publicly available datasets. We found 39 genes with potential oncogenic features (category A) and 17 genes that may function such as tumor suppressors (category D). We showed that pharmacologically targeting the dynamin-related GTPase OPA1 identified in category A successfully suppresses various pancreatic cancer phenotypes. These phenotypes include cell proliferation in both 2D and 3D cultures, cell migration, mitochondrial bioenergetics, and alterations in mitochondrial morphology and dynamics. Our data support and extend a previous study that reported genetic OPA1 knockdown using siRNAs suppresses spheroid growth and anchorage-independent growth in PANC-1 cells.[35] Furthermore, we show that the inhibition of OPA1 produces a synergistic effect when combined with a mutation-specific KRAS inhibitor, significantly reducing cell proliferation and spheroid growth. Our findings propose a therapeutic approach for treating cancer by simultaneously targeting mitochondrial function and KRAS signaling.

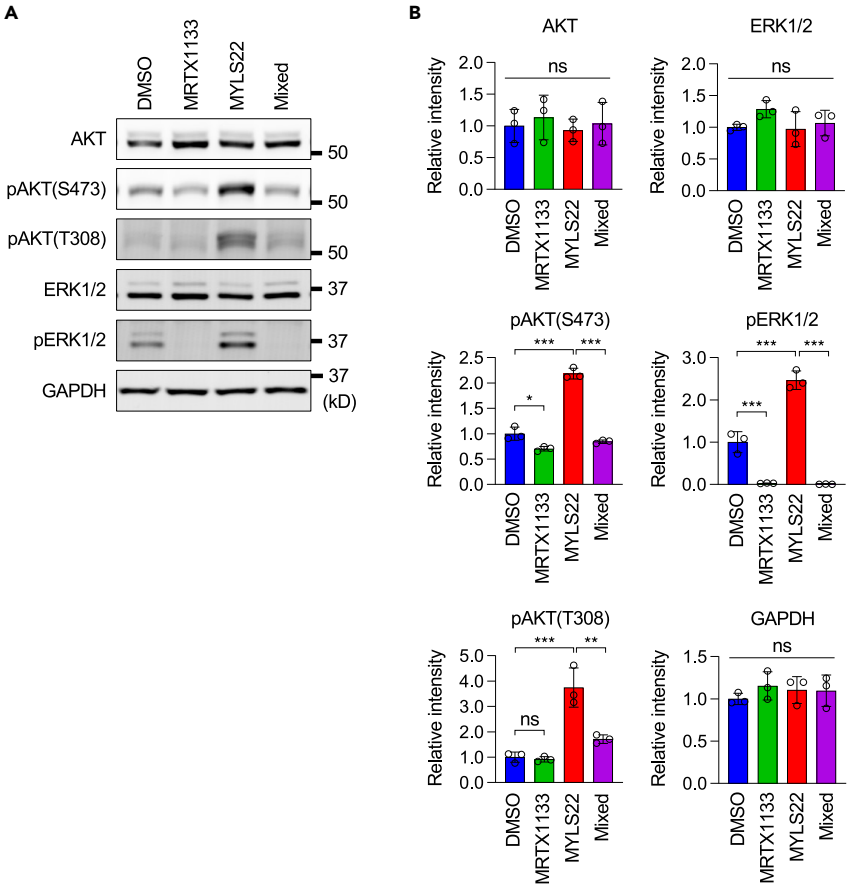

Figure 7. MYLS22 promotes the phosphorylation of AKT and ERK in a KRAS-dependent manner

(A) PANC-1 cells were treated with DMSO, MRTX1133, MYLS22, or both for 24 h. Whole-cell lysates were subjected to Western blotting using the indicated antibodies.

(B) Quantification of band intensity (mean ± SD, $n = 3$). ANOVA with post-hoc Tukey: *$p < 0.05$, **$p < 0.01$, ***$p < 0.001$.

Mitochondria are dynamic organelles that actively fuse and divide to regulate their structure.[21,36–38] Mitochondrial fusion is controlled by inner-membrane-located OPA1 and outer-membrane-located GTPases, mitofusins.[21] In contrast, division is mediated by another GTPase, DRP1. During KRAS-driven oncogenic transformation, the mitochondrial division is upregulated, resulting in smaller mitochondria.[28,29] This may suggest that further tilting the balance between fusion and division against fusion critically decreases mitochondrial functional competence. Interestingly, however, we found that the inhibition of mitochondrial fusion by knocking down MFN1 causes the fragmentation of mitochondria but does not inhibit cell proliferation in PANC-1 cells. Therefore, PANC-1 cells appear to be independent of mitochondrial fusion for their proliferation. Instead, our data suggest that inner membrane cristae are important for pancreatic cancer cell proliferation. Since cristae are involved in multiple processes in mitochondria including ATP production, metabolic reprogramming, and ROS production, it would be of great interest to further define the role of cristae in pancreatic cancer. Supporting this notion, we found that MYLS22 inhibits OCRs in PANC-1 cells.

Another pathway enriched in category A is mitochondrial translation. Mitochondrial energy production is critical for the proliferation of pancreatic cancer, even though glycolysis is enhanced. Therefore, enhanced mitochondrial translation may help produce cellular ATP to support the high energy demands of rapidly proliferating cancer cells, even under conditions where glycolysis is also upregulated. However, we found that chloramphenicol, which inhibits mitochondrial translation, suppresses the growth of MIA PaCa-2 cells but not PANC-1 cells. Our findings suggest that the potential oncogenic roles of mitochondrial translation may be specific to subpopulations of pancreatic cancer cells.

Components associated with mitochondrial gene expression are enriched as potential tumor suppressors in category D. These components can also affect mitochondrial energy production and metabolism. One possibility that explains this enrichment is that specific metabolic pathways or bioenergetic intermediates play a crucial role in tumor suppression. Alternatively, mitochondrial gene expression can affect nuclear gene expression for tumor suppressor genes through their inter-organelle crosstalk.[39] In future studies, we are interested in defining specific mechanisms that could affect pancreatic cancer through this pathway.

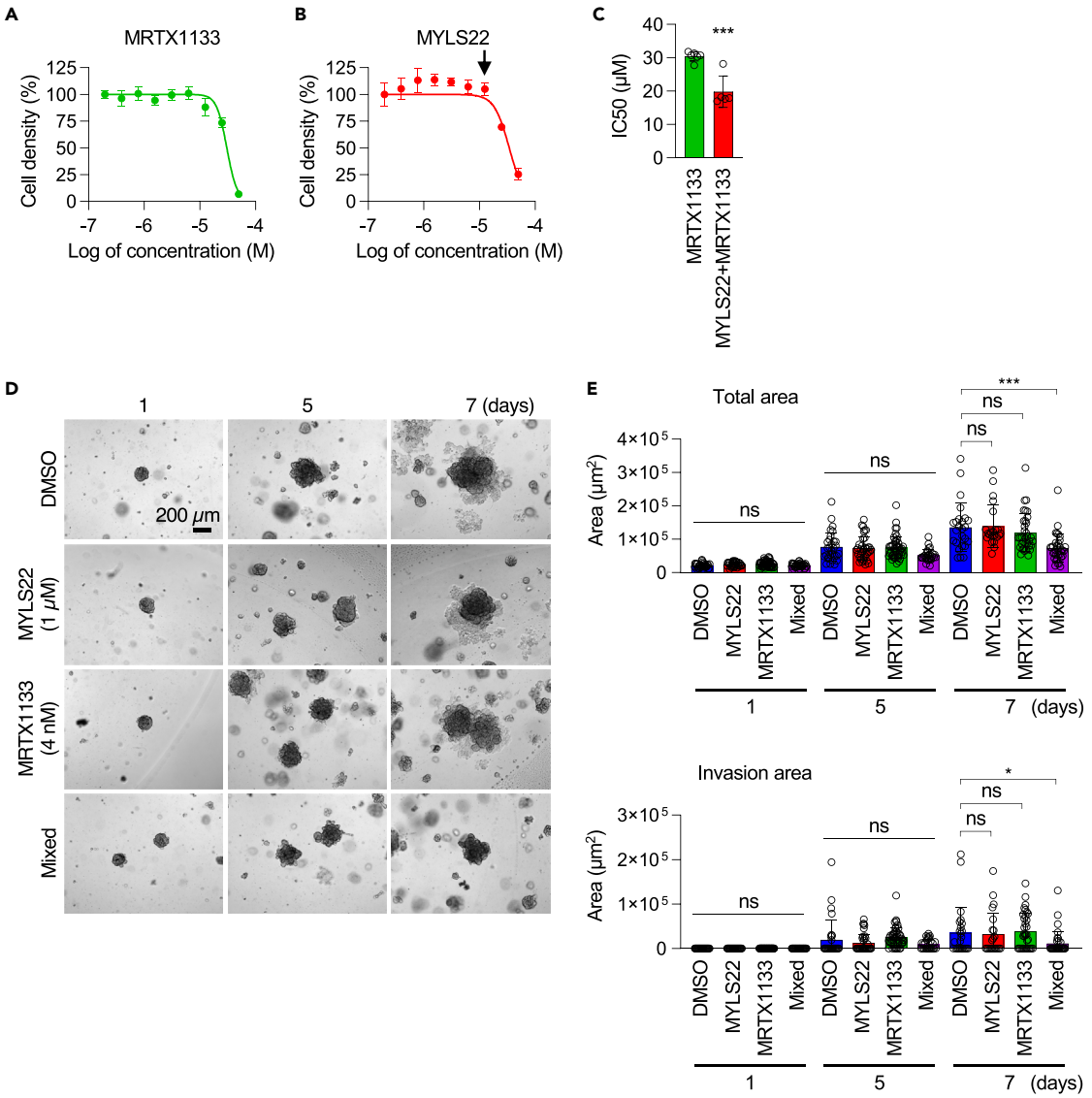

Figure 8. Synergistic effects of MRTX1133 and MYLS22 on cell proliferation and spheroid growth

(A and B) PANC-1 cells were cultured with 0–50 μM of MRTX1133 (A) or MYLS22 (B) for 72 h. Cell density was assessed using a crystal violet assay (mean ± SD, $n = 5$).

(C) The IC_{50} of MRTX1133 for cell proliferation was evaluated in the presence or absence of a sub-effective concentration of MYLS22 (12.5 μM, indicated by an arrow in panel B) (mean ± SD, $n = 5$).

(D) Spheroid growth. Spheroids of PANC-1 cells were cultured in Geltrex for 7 days in the presence or absence of 4 nM MRTX1133 and/or 1 μM MYLS22.

(E) Quantification of the total and invasion areas (mean ± SD, $n > 20$). Student's t-test in (C) and ANOVA with post-hoc Tukey in (E): $*p < 0.05$, $***p < 0.001$.

The potential of mCAUSE extends beyond pancreatic cancers. It has the potential to map the landscape of mitochondrial proteins that may be inhibited to control cancer cell phenotypes *in vitro* and *in vivo* across various types of cancers. Considering the existence of around 30 different cancer types, mCAUSE offers a promising navigational tool. It can effectively prioritize potential targets for cancer treatment, filtering through the extensive combinations of mitochondrial proteins and cancer types. This method, therefore, represents a significant stride forward in personalized cancer therapy and offers a wide array of future research and clinical applications.

Limitations of the study

In the current work, our investigation was limited to an *in vitro* culture system. Extending our findings to animal models to explore tumor mitigation *in vivo* would be of great interest. Additionally, testing the efficacy of targeting mitochondrial structure and dynamics alongside KRAS in human primary tumors represents another crucial future direction. Such investigations could potentially lead to the development of

therapeutic strategies that control mitochondrial bioenergetics and intracellular signaling in this devastating cancer. Beyond pancreatic cancer, we aim to extend mCAUSE to other, and possibly all, cancer types to identify effective mitochondrial targets for treating each one.

RESOURCE AVAILABILITY

Lead contact

Further information and requests for resources should be directed to and will be fulfilled by the lead contact, Hiromi Sesaki (hsesaki@jhmi.edu).

Materials availability

Cell lines and plasmids constructed in this study are available from the lead contact upon request.

Data and code availability

- All data reported in this article will be shared by the lead contact upon request.
- This article does not report original code.
- Any additional information required to reanalyze the data reported in this article is available from the lead contact upon request.

ACKNOWLEDGMENTS

We thank members of the Iijima and Sesaki labs for invaluable discussions and technical assistance. We are also grateful to Dr. Lei Zheng for his insightful and valuable comments on the article. This work was supported by NIH grants to MI (GM131768), AJE (U54CA26808), and HS (GM144103) by a Black in Cancer/Emerald Foundation Postdoctoral Fellowship to JJW, a Breast Cancer Research Foundation (BCRF-22-048) grant to AJE, and a Sol Goldman Pancreatic Cancer Research Grant to HS.

AUTHOR CONTRIBUTIONS

DM, FI, WI, MI, and HS designed the study. DM, FI, GT, and WI performed experiments. DM, FI, WI, NY, XW, JJW, AJE, MI, and HS analyzed and discussed data. DM, FI, WI, GT, NY, MI, and HS wrote and reviewed the article.

DECLARATION OF INTERESTS

AJE has unlicensed patents related to keratin 14 as a prognostic marker and antibody strategy for anti-cancer therapeutics. AJE is a consultant for BioNTech. AJE's spouse is an employee of ImmunoCore.

STAR★METHODS

Detailed methods are provided in the online version of this paper and include the following:

- KEY RESOURCES TABLE
- EXPERIMENTAL MODEL AND STUDY PARTICIPANT DETAILS
  - Cells
- METHOD DETAILS
  - Data analysis
  - Inhibitors
  - Cell proliferation
  - Spheroid growth
  - Wound-healing assay
  - Western blotting
  - Laser confocal immunofluorescence microscopy
  - Mitochondrial fusion
  - Electron microscopy
  - Plasmids
  - Lentivirus
  - Mitochondrial respiration
  - Glycolysis
- QUANTIFICATION AND STATISTICAL ANALYSIS

SUPPLEMENTAL INFORMATION

Supplemental information can be found online at https://doi.org/10.1016/j.isci.2024.110880.

Received: January 11, 2024
Revised: August 12, 2024
Accepted: September 2, 2024
Published: September 3, 2024

REFERENCES

1. Collisson, E.A., Bailey, P., Chang, D.K., and Biankin, A.V. (2019). Molecular subtypes of pancreatic cancer. Nat. Rev. Gastroenterol. Hepatol. *16*, 207–220. https://doi.org/10.1038/s41575-019-0109-y.
2. Buscail, L., Bournet, B., and Cordelier, P. (2020). Role of oncogenic KRAS in the diagnosis, prognosis and treatment of pancreatic cancer. Nat. Rev. Gastroenterol. Hepatol. *17*, 153–168. https://doi.org/10.1038/s41575-019-0245-4.
3. Hayashi, A., Hong, J., and Iacobuzio-Donahue, C.A. (2021). The pancreatic cancer genome revisited. Nat. Rev. Gastroenterol. Hepatol. *18*, 469–481. https://doi.org/10.1038/s41575-021-00463-z.
4. Park, W., Chawla, A., and O'Reilly, E.M. (2021). Pancreatic Cancer: A Review. JAMA *326*, 851–862. https://doi.org/10.1001/jama.2021.13027.
5. Hosein, A.N., Dougan, S.K., Aguirre, A.J., and Maitra, A. (2022). Translational advances in pancreatic ductal adenocarcinoma therapy. Nat. Can. (Ott.) *3*, 272–286. https://doi.org/10.1038/s43018-022-00349-2.
6. Mizrahi, J.D., Surana, R., Valle, J.W., and Shroff, R.T. (2020). Pancreatic cancer. Lancet *395*, 2008–2020. https://doi.org/10.1016/S0140-6736(20)30974-0.
7. Siegel, R.L., Miller, K.D., Fuchs, H.E., and Jemal, A. (2021). Cancer Statistics, 2021. CA A Cancer J. Clin. *71*, 7–33. https://doi.org/10.3322/caac.21654.
8. Encarnación-Rosado, J., and Kimmelman, A.C. (2021). Harnessing metabolic dependencies in pancreatic cancers. Nat. Rev. Gastroenterol. Hepatol. *18*, 482–492. https://doi.org/10.1038/s41575-021-00431-7.
9. Camelo, F., and Le, A. (2021). The Intricate Metabolism of Pancreatic Cancers. Adv. Exp. Med. Biol. *1311*, 77–88. https://doi.org/10.1007/978-3-030-65768-0_5.
10. Vaziri-Gohar, A., Zarei, M., Brody, J.R., and Winter, J.M. (2018). Metabolic Dependencies in Pancreatic Cancer. Front. Oncol. *8*, 617. https://doi.org/10.3389/fonc.2018.00617.
11. Viale, A., Pettazzoni, P., Lyssiotis, C.A., Ying, H., Sánchez, N., Marchesini, M., Carugo, A., Green, T., Seth, S., Giuliani, V., et al. (2014). Oncogene ablation-resistant pancreatic cancer cells depend on mitochondrial function. Nature *514*, 628–632. https://doi.org/10.1038/nature13611.
12. Siolas, D., Morrissey, C., and Oberstein, P.E. (2020). The Achilles' Heel of Pancreatic Cancer: Targeting pancreatic cancer's unique immunologic characteristics and metabolic dependencies in clinical trials. J. Pancreatol. *3*, 121–131. https://doi.org/10.1097/JP9.0000000000000052.
13. Rath, S., Sharma, R., Gupta, R., Ast, T., Chan, C., Durham, T.J., Goodman, R.P., Grabarek, Z., Haas, M.E., Hung, W.H.W., et al. (2021). MitoCarta3.0: an updated mitochondrial proteome now with sub-organelle localization and pathway annotations. Nucleic Acids Res. *49*, D1541–D1547. https://doi.org/10.1093/nar/gkaa1011.
14. Cancer Genome Atlas Research Network, Weinstein, J.N., Collisson, E.A., Mills, G.B., Shaw, K.R.M., Ozenberger, B.A., Ellrott, K., Shmulevich, I., Sander, C., and Stuart, J.M. (2013). The Cancer Genome Atlas Pan-Cancer analysis project. Nat. Genet. *45*, 1113–1120. https://doi.org/10.1038/ng.2764.
15. Tang, G., Cho, M., and Wang, X. (2022). OncoDB: an interactive online database for analysis of gene expression and viral infection in cancer. Nucleic Acids Res. *50*, D1334–D1339. https://doi.org/10.1093/nar/gkab970.
16. Herkenne, S., Ek, O., Zamberlan, M., Pellattiero, A., Chergova, M., Chivite, I., Novotná, E., Rigoni, G., Fonseca, T.B., Samardzic, D., et al. (2020). Developmental and Tumor Angiogenesis Requires the Mitochondria-Shaping Protein Opa1. Cell Metabol. *31*, 987–1003.e8. https://doi.org/10.1016/j.cmet.2020.04.007.
17. Zamberlan, M., Boeckx, A., Muller, F., Vinelli, F., Ek, O., Vianello, C., Coart, E., Shibata, K., Christian, A., Grespi, F., et al. (2022). Inhibition of the mitochondrial protein Opa1 curtails breast cancer growth. J. Exp. Clin. Cancer Res. *41*, 95. https://doi.org/10.1186/s13046-022-02304-6.
18. Jin, L., Li, D., Alesi, G.N., Fan, J., Kang, H.B., Lu, Z., Boggon, T.J., Jin, P., Yi, H., Wright, E.R., et al. (2015). Glutamate dehydrogenase 1 signals through antioxidant glutathione peroxidase 1 to regulate redox homeostasis and tumor growth. Cancer Cell *27*, 257–270. https://doi.org/10.1016/j.ccell.2014.12.006.
19. Hu, C.M., Yeh, M.T., Tsao, N., Chen, C.W., Gao, Q.Z., Chang, C.Y., Lee, M.H., Fang, J.M., Sheu, S.Y., Lin, C.J., et al. (2012). Tumor cells require thymidylate kinase to prevent dUTP incorporation during DNA repair. Cancer Cell *22*, 36–50. https://doi.org/10.1016/j.ccr.2012.04.038.
20. Becattini, B., Sareth, S., Zhai, D., Crowell, K.J., Leone, M., Reed, J.C., and Pellecchia, M. (2004). Targeting apoptosis via chemical design: inhibition of bid-induced cell death by small organic molecules. Chem. Biol. *11*, 1107–1117. https://doi.org/10.1016/j.chembiol.2004.05.022.
21. Murata, D., Arai, K., Iijima, M., and Sesaki, H. (2020). Mitochondrial division, fusion and degradation. J. Biochem. *167*, 233–241. https://doi.org/10.1093/jb/mvz106.
22. Bannwarth, S., Ait-El-Mkadem, S., Chaussenot, A., Genin, E.C., Lacas-Gervais, S., Fragaki, K., Berg-Alonso, L., Kageyama, Y., Serre, V., Moore, D.G., et al. (2014). A mitochondrial origin for frontotemporal dementia and amyotrophic lateral sclerosis through CHCHD10 involvement. Brain *137*, 2329–2345. https://doi.org/10.1093/brain/awu138.
23. Nagdas, S., Kashatus, J.A., Nascimento, A., Hussain, S.S., Trainor, R.E., Pollock, S.R., Adair, S.J., Michaels, A.D., Sesaki, H., Stelow, E.B., et al. (2019). Drp1 Promotes KRas-Driven Metabolic Changes to Drive Pancreatic Tumor Growth. Cell Rep. *28*, 1845–1859.e5. https://doi.org/10.1016/j.celrep.2019.07.031.
24. Stephan, T., Brüser, C., Deckers, M., Steyer, A.M., Balzarotti, F., Barbot, M., Behr, T.S., Heim, G., Hübner, W., Ilgen, P., et al. (2020). MICOS assembly controls mitochondrial inner membrane remodeling and crista junction redistribution to mediate cristae formation. EMBO J. *39*, e104105. https://doi.org/10.15252/embj.2019104105.
25. Kozjak-Pavlovic, V. (2017). The MICOS complex of human mitochondria. Cell Tissue Res. *367*, 83–93. https://doi.org/10.1007/s00441-016-2433-7.
26. Ikeda, H., Muroi, M., Kondoh, Y., Ishikawa, S., Kakeya, H., Osada, H., and Imoto, M. (2020). Miclxin, a Novel MIC60 Inhibitor, Induces Apoptosis via Mitochondrial Stress in beta-Catenin Mutant Tumor Cells. ACS Chem. Biol. *15*, 2195–2204. https://doi.org/10.1021/acschembio.0c00381.
27. Padmanaban, V., Krol, I., Suhail, Y., Szczerba, B.M., Aceto, N., Bader, J.S., and Ewald, A.J. (2019). E-cadherin is required for metastasis in multiple models of breast cancer. Nature *573*, 439–444. https://doi.org/10.1038/s41586-019-1526-3.
28. Serasinghe, M.N., Wieder, S.Y., Renault, T.T., Elkholi, R., Asciolla, J.J., Yao, J.L., Jabado, O., Hoehn, K., Kageyama, Y., Sesaki, H., and Chipuk, J.E. (2015). Mitochondrial Division Is Requisite to RAS-Induced Transformation and Targeted by Oncogenic MAPK Pathway Inhibitors. Mol. Cell *57*, 521–536. https://doi.org/10.1016/j.molcel.2015.01.003.
29. Kashatus, J.A., Nascimento, A., Myers, L.J., Sher, A., Byrne, F.L., Hoehn, K.L., Counter, C.M., and Kashatus, D.F. (2015). Erk2 phosphorylation of Drp1 promotes mitochondrial fission and MAPK-driven tumor growth. Mol. Cell *57*, 537–551. https://doi.org/10.1016/j.molcel.2015.01.002.
30. Hoxhaj, G., and Manning, B.D. (2020). The PI3K-AKT network at the interface of oncogenic signalling and cancer metabolism. Nat. Rev. Cancer *20*, 74–88. https://doi.org/10.1038/s41568-019-0216-7.
31. Caunt, C.J., Sale, M.J., Smith, P.D., and Cook, S.J. (2015). MEK1 and MEK2 inhibitors and cancer therapy: the long and winding road. Nat. Rev. Cancer *15*, 577–592. https://doi.org/10.1038/nrc4000.
32. Quirós, P.M., Mottis, A., and Auwerx, J. (2016). Mitonuclear communication in homeostasis and stress. Nat. Rev. Mol. Cell Biol. *17*, 213–226. https://doi.org/10.1038/nrm.2016.23.
33. Pakos-Zebrucka, K., Koryga, I., Mnich, K., Ljujic, M., Samali, A., and Gorman, A.M. (2016). The integrated stress response. EMBO Rep. *17*, 1374–1395. https://doi.org/10.15252/embr.201642195.
34. Hallin, J., Bowcut, V., Calinisan, A., Briere, D.M., Hargis, L., Engstrom, L.D., Laguer, J., Medwid, J., Vanderpool, D., Lifset, E., et al. (2022). Anti-tumor efficacy of a potent and selective non-covalent KRASG12D inhibitor. Nat. Med. *28*, 2171–2182. https://doi.org/10.1038/s41591-022-02007-7.
35. Carmona-Carmona, C.A., Dalla Pozza, E., Ambrosini, G., Cisterna, B., Palmieri, M., Decimo, I., Cuezva, J.M., Bottani, E., and Dando, I. (2022). Mitochondrial Elongation and OPA1 Play Crucial Roles during the Stemness Acquisition Process in Pancreatic Ductal Adenocarcinoma. Cancers *14*, 3432. https://doi.org/10.3390/cancers14143432.
36. Friedman, J.R., and Nunnari, J. (2014). Mitochondrial form and function. Nature *505*, 335–343. https://doi.org/10.1038/nature12985.
37. Youle, R.J., and van der Bliek, A.M. (2012). Mitochondrial fission, fusion, and stress. Science *337*, 1062–1065. https://doi.org/10.1126/science.1219855.
38. Mishra, P., and Chan, D.C. (2016). Metabolic regulation of mitochondrial dynamics. J. Cell Biol. *212*, 379–387. https://doi.org/10.1083/jcb.201511036.

39. Walker, B.R., and Moraes, C.T. (2022). Nuclear-Mitochondrial Interactions. Biomolecules *12*, 427. https://doi.org/10.3390/biom12030427.

40. Sarbassov, D.D., Guertin, D.A., Ali, S.M., and Sabatini, D.M. (2005). Phosphorylation and regulation of Akt/PKB by the rictor-mTOR complex. Science *307*, 1098–1101.

41. Stewart, S.A., Dykxhoorn, D.M., Palliser, D., Mizuno, H., Yu, E.Y., An, D.S., Sabatini, D.M., Chen, I.S., Hahn, W.C., Sharp, P.A., et al. (2003). Lentivirus-delivered stable gene silencing by RNAi in primary cells. RNA *9*, 493–501.

42. Patterson, G.H., and Lippincott-Schwartz, J. (2002). A photoactivatable GFP for selective photolabeling of proteins and cells. Science *297*, 1873–1877.

43. GTEx Consortium (2013). The Genotype-Tissue Expression (GTEx) project. Nat. Genet. *45*, 580–585. https://doi.org/10.1038/ng.2653.

44. Murata, D., Yamada, T., Tokuyama, T., Arai, K., Quirós, P.M., López-Otín, C., Iijima, M., and Sesaki, H. (2020). Mitochondrial Safeguard: a stress response that offsets extreme fusion and protects respiratory function via flickering-induced Oma1 activation. EMBO J. *39*, e105074. https://doi.org/10.15252/embj.2020105074.

45. Adachi, Y., Itoh, K., Yamada, T., Cerveny, K.L., Suzuki, T.L., Macdonald, P., Frohman, M.A., Ramachandran, R., Iijima, M., and Sesaki, H. (2016). Coincident Phosphatidic Acid Interaction Restrains Drp1 in Mitochondrial Division. Mol. Cell *63*, 1034–1043. https://doi.org/10.1016/j.molcel.2016.08.013.

46. Murata, D., Roy, S., Lutsenko, S., Iijima, M., and Sesaki, H. (2024). Slc25a3-dependent copper transport controls flickering-induced Opa1 processing for mitochondrial safeguard. Dev. Cell. https://doi.org/10.1016/j.devcel.2024.06.008.

47. Kageyama, Y., Hoshijima, M., Seo, K., Bedja, D., Sysa-Shah, P., Andrabi, S.A., Chen, W., Höke, A., Dawson, V.L., Dawson, T.M., et al. (2014). Parkin-independent mitophagy requires Drp1 and maintains the integrity of mammalian heart and brain. EMBO J. *33*, 2798–2813. https://doi.org/10.15252/embj.201488658.

STAR★METHODS

KEY RESOURCES TABLE

REAGENT or RESOURCE	SOURCE	IDENTIFIER
Antibodies		
Mouse monoclonal anti-PDH	Abcam	Cat# ab110333; RRID: AB_10862029
Rabbit polyclonal anti-MFN1	Proteintech	Cat# 13798-1-AP; RRID: AB_2266318
Mouse monoclonal anti-GAPDH	Thermo Fisher Scientific	Cat# MA5-15738; RRID: AB_10977387
Mouse monoclonal anti-DRP1	BD Biosciences	Cat# 611113; RRID:AB_398424
Rabbit polyclonal anti-TOM20	Proteintech	Cat# 11802-1-AP; RRID: AB_2207530
Rabbit polyclonal anti-MIC60	Proteintech	Cat# 10179-1-AP; RRID: AB_2127193
Rabbit polyclonal anti-AKT	Cell Signaling Technology	Cat# 9272; RRID: AB_329827
Rabbit monoclonal anti-pAKT(S473)	Cell Signaling Technology	Cat# 4060; RRID: AB_2315049
Rabbit monoclonal anti-pAKT(T308)	Cell Signaling Technology	Cat# 2965; RRID: AB_2255933
Mouse monoclonal anti-ERK1/2	Cell Signaling Technology	Cat#9107; RRID: AB_10695739
Rabbit monoclonal anti-pERK1/2	Cell Signaling Technology	Cat#4370; RRID: AB_2315112
Alexa 488-conjugated anti-mouse IgG	Thermo Fisher Scientific	Cat# A21202; RRID: AB_141607
Alexa 488-conjugated anti-rabbit IgG	Thermo Fisher Scientific	Cat# A21206; RRID: AB_2535792
Alexa 568-conjugated anti-rabbit IgG	Thermo Fisher Scientific	Cat# A10042; RRID: AB_2534017
Alexa 647-conjugated anti-rabbit IgG	Thermo Fisher Scientific	Cat# A31573; RRID: AB_2536183
Chemicals, peptides, and recombinant proteins		
Dulbecco's Modified Eagle's Medium (DMEM) – high glucose	Sigma-Aldrich	Cat# D5796
Fetal Bovine Serum (FBS)	Corning	Cat# 35-010-CV
DPBS	Corning	Cat# 21-031-CV
0.05% Trypsin-EDTA	Gibco	Cat# 25300-054
DMSO	Corning	Cat# 25-950-CQC
Chloramphenicol	Sigma-Aldrich	Cat# C0378-5G
MYLS22	Med Chem Express	Cat# HY-136446
R162	Caymen	Cat# 30922
YMU1	Caymen	Cat# 21981
BI-6C9	Santa Cruz Biotechnology	Cat# sc-210915
AP5A	Santa Cruz Biotechnology	Cat# sc-204156
Fidarestat	Med Chem Express	Cat# HY-105185
ML348	Med Chem Express	Cat# HY-100736
FC9402	Med Chem Express	Cat# HY-141552
Miclxin	Med Chem Express	Cat# HY-138301
MRTX1133	Fisher Scientific	Cat# NC2083191
Crystal violet	Sigma-Aldrich	Cat# 65092A-95
Acetic acid	Thermo Fisher Scientific	Cat# A38-212
Paraformaldehyde	Sigma-Aldrich	Cat# P6148
Triton X-100	Sigma-Aldrich	Cat# T9284
BSA	Sigma-Aldrich	Cat# A7906
Alexa 568-conjugated phalloidin	Thermo Fisher Scientific	Cat# A12380
DAPI	Roche	Cat# 10236276001
Phusion High-Fidelity DNA Polymerase	NEB	Cat# M0530

(*Continued on next page*)

Continued

REAGENT or RESOURCE	SOURCE	IDENTIFIER
Quick Ligation Kit	NEB	Cat# M2200
Lipofectamine 2000 Transfection Reagent	Thermo Fisher Scientific	Cat# 11668019
Lipofectamine RNAiMAX Transfection Reagent	Thermo Fisher Scientific	Cat# 13778150
Polybrene Infection/Transfection Reagent	MilliporeSigma	Cat# TR-1003-G
Tetramethylrhodamine, ethyl ester (TMRE)	Thermo Fisher Scientific	Cat# T669
Sodium cacodylate, trihydrate	Electron Microscopy Sciences	Cat# 12300
25% glutaraldehyde	Electron Microscopy Sciences	Cat# 16220
4% Osmium Tetroxide (OsO_4)	Electron Microscopy Sciences	Cat# 19190
Potassium hexacyanoferrate(II), trihydrate	Sigma-Aldrich	Cat# P3289
Uranyl acetate	Ted Pella, Inc.	Cat# 19481
EMBED 812 RESIN	Electron Microscopy Sciences	Cat# 14900
DDSA	Electron Microscopy Sciences	Cat# 13710
NMA	Electron Microscopy Sciences	Cat# 19000
DMP-30	Electron Microscopy Sciences	Cat# 13600
RIPA Buffer (10X)	Cell Signaling Technology	Cat# 9806S
cOmplete, Mini, EDTA-free Protease Inhibitor Cocktail	Roche	Cat# 11836170001
Phosphatase Inhibitor Cocktail 2	Sigma-Aldrich	Cat# P5726
Phosphatase Inhibitor Cocktail 3	Sigma-Aldrich	Cat# P0044
Tween 20	Sigma-Aldrich	Cat# P7949
4–20% Criterion TGX Precast Gels	Bio-Rad Laboratories	Cat# 5671095
Seahorse XF Base Medium Minimal DMEM	Agilent	Cat# 102353-100
L-Glutamine (200 mM)	Gibco	Cat# 25030081
Sodium pyruvate (100 mM)	Sigma-Aldrich	Cat# S8636
D-Glucose	Sigma-Aldrich	Cat# G7021
Oligomycin	Sigma-Aldrich	Cat# O4876
FCCP	Sigma-Aldrich	Cat# C2920
Antimycin A	Sigma-Aldrich	Cat# A8674
Rotenone	Sigma-Aldrich	Cat# R8875
2-Deoxy-D-glucose	MilliporeSigma	Cat# 25972-1GM
Methylcellulose	Sigma-Aldrich	Cat# M0512
Geltrex	Thermo Fisher Scientific	Cat# A1413202
Critical commercial assays		
Seahorse XFe96/XF Pro FluxPak	Agilent	Cat# 103792-100
Experimental models: Cell lines		
Human: Panc-1 cells	ATCC	CRL-1469
Human: HEK293T cells	ATCC	CRL-3216
Oligonucleotides		
siRNA: Negative control	Thermo Fisher Scientific	Cat# 4390843
siRNA: MFN1 #1	Thermo Fisher Scientific	Assay ID: s31218
siRNA: MFN1 #2	Thermo Fisher Scientific	Assay ID: s31220
siRNA: MIC60 #1	Thermo Fisher Scientific	Assay ID: s21633
siRNA: MIC60 #2:	Thermo Fisher Scientific	Assay ID: s21634
shRNA targeting sequence: scramble: CCTAAGGTTAAGTCGCCCTCG	Sarbassov et al.[40]	Addgene Plasmid #1864

(*Continued on next page*)

Continued

REAGENT or RESOURCE	SOURCE	IDENTIFIER
shRNA targeting sequence: DRP1: GCTACTTTACTCCAACTTATT	Sigma-Aldrich	TRCN0000001097
Recombinant DNA		
pHR-CMV8.2ΔR	Stewart et al.[41]	Addgene Plasmid #8455
pCMV-VSVG	Stewart et al.[41]	Addgene Plasmid #8454
pPAGFP-N1	Patterson et al.[42]	Addgene Plasmid #11909
pHR-SIN Su9-PAGFP	This paper	N/A
pLKO.1 scrambled shRNA	This paper	N/A
pLKO.1 DRP1 shRNA	This paper	N/A
Software and algorithms		
MitoCarta3.0	Rath et al., 2021[13]	www.broadinstitute.org/mitocarta
OncoDB	Tang et al., 2022[15]	https://oncodb.org
GTEx database	Consortium, 2013[43]	https://gtexportal.org/home/
FIJI	NIH	https://imagej.net/software/fiji/downloads
Prism	GraphPad	https://www.graphpad.com/features
Seahorse Wave Controller Software	Agilent	https://www.agilent.com/en/product/cell-analysis/real-time-cell-metabolic-analysis/xf-software/seahorse-wave-controller-software-2-6-1-740904

EXPERIMENTAL MODEL AND STUDY PARTICIPANT DETAILS

Cells

PANC-1 and MIA PaCa-2 cells were obtained from the American Type Culture Collection and were cultured in Dulbecco's Modified Eagle Medium (DMEM) containing 10% fetal bovine serum. For siRNA knockdown, PANC-1 cells were plated at a density of 100,000 cells/well in a 6-well plate and cultured for 24 h. The cells were transfected with siRNAs at 10 nM using Lipofectamine RNAiMAX (Invitrogen). The following Silencer Select siRNAs from Thermo Fisher were used: negative control (4390843), MFN1 #1 (s31218), MFN1 #2 (s31220), MIC60 #1 (s21633), and MIC60 #2 (s21634).

METHOD DETAILS

Data analysis

We selected 1136 mito-genes that encode mitochondrial proteins based on MitoCarta3.0.[13] Using OncoDB,[15] we retrieved gene expression profiles of these genes from pancreatic cancer samples in TCGA[14] and normal pancreas tissues in the GTEx database.[43] We employed Student's t-test followed by the Benjamini-Hochberg procedure to calculate adjusted p-values. For the survival analysis of pancreatic cancer, we applied the Kaplan-Meier model to estimate the survival probabilities along with the survival time. Based on RNA expression, we categorized the cancer cases into 'high' or 'low' expression groups using a median 50% threshold. We then used the log-rank test to compare the survival curves between these two groups. Additionally, we employed the Cox regression analysis to determine the hazard ratio associated with the expression levels of the selected genes. GO enrichment analysis of differentially expressed genes was carried out using PANTHER, and statistical significance was adjusted using Bonferroni correction. Biological processes that met the criteria of a p-value less than 0.05 and showed gene enrichment greater than 20-fold are presented.

Inhibitors

Chloramphenicol (C0378-5G, Sigma), MYLS22 (HY-136446, Med Chem Express), R162 (30922, Cayman), YMU1 (21981, Cayman), BI-6C9 (sc-210915, Santa Cruz Biotechnology), AP5A (sc-204156, Santa Cruz Biotechnology), Fidarestat (HY-105185, Med Chem Express), ML348 (HY-100736, Med Chem Express), FC9402 (HY-141552, Med Chem Express), MRTX1133 (NC2083191, Fisher Scientific), and Miclxin (HY-138301, Med Chem Express) were used.

Cell proliferation

PANC-1 and MIA PaCa-2 cells were plated at 3,000 cells/well in a 96-well plate and incubated at 37°C with 5% CO_2 for 24 h. Cells were then treated with various inhibitors for 48 h. To determine IC_{50}, PANC-1 cells were plated at 3,000 cells/well at in a 96-well plate and incubated at 37°C with 5% CO_2 for 24 h. Cells were then treated with various inhibitors for 72 h. To examine the combined effect of DRP1 knockdown and

MYLS22, PANC-1 cells were seeded at 100,000 cells/well in a 6-well plate and cultured for 24 h. The cells were then incubated with lentiviruses expressing either scramble or DRP1 shRNA in DMEM containing 10% FBS and 8 μg/ml polybrene for 24 h. The cells were subsequently cultured in DMEM containing 10% FBS for an additional 3 days. The cells were then replated at 10,000 cells/well in a 96-well plate and cultured for 24 h before being treated with 50 μM MYLS22 for an additional 2 days. For the siRNA knockdown of MFN1 and MIC60, PANC-1 cells were plated at a density of 100,000 cells/well in a 6-well plate and cultured for 24 h. The cells were transfected with siRNAs at 10 nM using Lipofectamine RNAiMAX (Invitrogen). After 3 days, the cells were replated at a density of 10,000 cells/well in a 96-well plate and cultured for 24 h. The cells were then transfected with siRNAs again and cultured for an additional 2 days. For crystal violet staining, the cells were fixed with 4% paraformaldehyde in PBS at room temperature for 20 min. After washing with MilliQ water, cell densities were assessed by staining with 0.35% crystal violet (65092A-95, Sigma Aldrich) for 20 min. After washing three times with water and air-drying, 150 μl of 10% acetic acid was added, and the absorbance was measured at 595 nm using a multimode microplate reader (CLARIOstar, BMG Labtech).

Spheroid growth

PANC-1 cells were cultured in a 10-cm dish in DMEM containing 10% FBS. The cells were washed with PBS and detached from the dish using 2 ml of pre-warmed 0.05% trypsin-EDTA for 5 min. After adding 5 ml of the culture medium, the cells were centrifuged twice in a 15 ml conical tube at 1500 rpm for 3 min and then pelleted. The cells were resuspended at 10,000 cells/ml in 10 ml of the culture medium containing 0.24% methylcellulose. A 20 μl aliquot of the cell suspension was placed on the bottom of the lid of a 10-cm dish filled with PBS and incubated for 2–4 days in a cell culture incubator at 37°C with 5% CO_2 to allow spheroid formation.[27] The spheroids were suspended in 2–3 ml of culture medium and transferred to a 15 ml conical tube coated with 3% BSA in PBS, using a 10 ml pipette coated with 3% BSA in PBS. The spheroids were washed three times in the culture medium at 1500 rpm for 3 s each time and resuspended at a concentration of 1 spheroid/μl in Geltrex (A1413202, Thermo Fisher). A 50-μl volume of the spheroid suspension was placed in 24-well plates and incubated at 37°C for 30 min to allow the Geltrex to solidify. Subsequently, 1 ml of the culture medium was added. The spheroids were then cultured for 7 days in a cell culture incubator at 37°C with 5% CO_2. The culture medium was changed on day 3 or 4. Images of the spheroids were captured using phase-contrast microscopy (AXIO Observer Z1, Zeiss). The size of the total and their invasion area were calculated using NIH Fiji software.

Wound-healing assay

PANC-1 cells were seeded in a 12-well plate and cultured until they reached 100% confluence. A wound was created by scratching a line across the bottom of the dish through the confluent cell monolayer using a sterile P-200 pipette tip. The cells were then gently rinsed with PBS and treated with DMEM containing either DMSO or 50 μM MYLS22 for 72 h. Images were captured using phase-contrast microscopy (AXIO Observer Z1, Zeiss). The width of the scratches was measured using NIH Fiji software.

Western blotting

PANC-1 cells were harvested and lysed in RIPA buffer (9806S, Cell Signaling), supplemented with cOmplete, Mini, EDTA-free Protease Inhibitor Cocktail (11836170001, Roche) and Phosphatase Inhibitor Cocktail 2 and 3 (P5726 and P0044, Sigma Aldrich), while on ice.[44] The lysates were centrifuged at 16,000 g for 10 min at 4°C, and the supernatants were collected. Proteins were separated using SDS-PAGE and subsequently transferred onto Immobilon-FL Transfer Membranes (Millipore). These membranes were blocked with PBS-T (PBS containing 0.05% Tween 20) and 3% BSA at room temperature for 1 h and were incubated with primary antibodies in PBS-T containing 3% BSA at 4°C overnight. The antibodies used were MFN1 (13798-1-AP; Proteintech), DRP1 (611113; BD Biosciences), MIC60 (10179-1-AP; Proteintech), AKT (9272, Cell Signaling), phospho-AKT at S473 (4060, Cell Signaling), phospho-AKT at T308 (13038, Cell Signaling), ERK1/2 (9107, Cell Signaling), phospho-ERK1/2 (4370, Cell Signaling), and GAPDH (MA5-15738, Invitrogen). After washing the membranes three times in PBS-T, they were incubated with appropriate fluorescently labeled secondary antibodies at room temperature for 1 h. Following another three washes in PBS-T, fluorescence signals were detected using a Typhoon laser-scanner platform (Amersham).

Laser confocal immunofluorescence microscopy

PANC-1 cells were seeded at 20,000 cells/well in an 8-well chamber and cultured for 24 h. The cells were then incubated with 50 μM MYLS22 for an additional 24 h. Subsequently, the cells were fixed in pre-warmed (37°C) PBS containing 4% paraformaldehyde for 20 min.[44,45] After washing three times with PBS, the cells were permeabilized with PBS containing 0.1% Triton X-100 for 8 min. The cells were then washed three more times with PBS and blocked in PBS containing 0.5% BSA at room temperature for 1 h.[44,45] Next, the cells were incubated with anti-PDH antibody (1:300 dilution in PBS containing 0.5% BSA; ab110333, Abcam) or TOM20 (1:1,000 dilution in PBS containing 0.5% BSA; 11802-1-AP; Proteintech) at 4°C overnight. The cells were washed three times with PBS and incubated with Alexa 488-conjugated anti-mouse IgG (1:400 dilution in PBS; A21202, Thermo Fisher) and Alexa 568-conjugated phalloidin (1:500 dilution in PBS; A12380, Thermo Fisher) at room temperature for 1 h. Finally, the cells were again washed three times with PBS and stained with 1 μg/ml DAPI. Samples were observed using a Zeiss LSM800 GaAsP laser scanning confocal microscope.[44,45] Mitochondrial length was measured using NIH Fiji software.[44,45]

Mitochondrial fusion

Mitochondrial fusion was examined using matrix-targeted photoactivatable GFP (mitoPAGFP).[22] The matrix-targeted presequence from Su9 was fused to the N-terminus of photoactivatable GFP (Addgene #11909) and cloned into the lentiviral vector pHR-SIN.[22] Cells were infected

with lentiviral particles carrying mitoPAGFP. Fifteen minutes before observation, cells were stained with 5 nM TMRE to visualize the mitochondria. MitoPAGFP was photoactivated using 405 nm light at 50% power, with 25 repetitions, for a total of 2.5 seconds, in a small region measuring 16 μm^2. The imaging was performed using a Zeiss LSM800 GaAsP confocal microscope equipped with an environmentally controlled chamber. Images were captured at 15-min intervals over a 60-min period. The fluorescence intensity of mitoPAGFP in the photoactivated region was quantified using NIH Fiji software.

Electron microscopy

Cells were fixed by 2% glutaraldehyde, 3 mM $CaCl_2$ and 0.1 M cacodylate buffer, pH 7.4, for 1 h.[46] After washes, samples were post-fixed in 1% OsO_4, 1% potassium hexacyanoferrate, and 0.1 M cacodylate, pH 7.4, for 1 h on ice. After washes in water, samples were incubated in 2% uranyl acetate for 30 min on ice. After dehydration using 50, 70, 90, and 100% ethanol, samples were embedded in EPON resin. Ultrathin sections were obtained using a Reichert-Jung ultracut E, stained with 2% uranyl acetate and lead citrate, and viewed using a transmission electron microscope (H-7600; Hitachi) equipped with a dual CCD camera (Advanced Microscopy Techniques).

Plasmids

To generate shRNA plasmids, the following target sequences were cloned into pLKO.1. Scramble: CCTAAGGTTAAGTCGCCCTCG ctcgagCGAGGGCGACTTAACCTTAGG, DRP1: GCTACTTTACTCCAACTTATTctcgagAATAAGTTGGAGTAAAGTAGC.

Lentivirus

HEK293T cells were seeded at 1.5×10^6 cells in a 10-cm dish and cultured for 24 h. To produce lentiviruses, 3 μg of pLKO.1 carrying shRNAs was co-transfected into HEK293T cells along with 3 μg of pHR-CMV8.2ΔR and 0.3 μg of pCMV-VSVG using Lipofectamine 2000 (Invitrogen).[44,47] After 20–22 h, the culture medium was replaced with fresh medium. After an additional 24 h, the culture medium containing the released viruses was collected. For lentiviral transduction, PANC-1 cells were seeded at 1×10^5 cells/well in a 6-well plate and cultured for 24 h. Cells were then incubated with lentivirus in the cell culture medium containing 10% FBS and 8 μg/ml polybrene for 24 h.

Mitochondrial respiration

Mitochondrial OCRs were measured using an XF96 Extracellular Flux Analyzer (Seahorse Bioscience) as described in previous studies.[44,47] PANC-1 cells were seeded at 10,000 cells/well in an XF 96-well culture microplate and cultured for 24 h. The cells were then incubated with 50 μM MYLS22 for an additional 24 h. Subsequently, the cells were washed twice with an XF base medium supplemented with 50 μM MYLS22, 25 mM glucose, and 4 mM L-glutamine. The cells were then incubated at 37°C in a CO_2-free incubator for 1 h. OCR measurements were performed according to the manufacturer's instructions. Baseline OCR was recorded three times, after which 1.6 μg/ml oligomycin (OM), 1 μM FCCP, and 0.5 μM rotenone/antimycin A (AM+Rot) were sequentially injected into each well.

Glycolysis

Glycolysis was measured by analyzing ECARs using an XF96 Extracellular Flux Analyzer (Seahorse Bioscience). PANC-1 cells were seeded at 10,000 cells/well in an XF 96-well culture microplate and cultured for 24 h. The cells were then incubated with 50 μM MYLS22 for an additional 24 h. Subsequently, the cells were washed twice with XF base medium supplemented with 50 μM MYLS22 and 4 mM L-glutamine and then incubated at 37°C in a CO_2-free incubator for 1 h. ECAR measurements were performed according to the manufacturer's instructions. Non-glycolytic acidification was recorded three times, after which 10 mM glucose, 1.6 μg/ml oligomycin, and 50 mM 2-deoxyglucose (2-DG) were sequentially injected into each well.

QUANTIFICATION AND STATISTICAL ANALYSIS

Statistical analysis was performed using GraphPad Prism 7. Student's t-test, ANOVA followed by post-hoc Tukey test or Šídák's test were used: *$p < 0.05$, **$p < 0.01$, ***$p < 0.001$. Specific statistical tests and significance thresholds are detailed in the figure legends.